Absorbing discretization effects with a massive renormalization scheme: The charm-quark mass

L. Del Debbio,[1] F. Erben,[2] J. M. Flynn,[3] R. Mukherjee,[3] and J. T. Tsang[2,*]

(RBC and UKQCD Collaborations)

[1]*Higgs Centre for Theoretical Physics, School of Physics and Astronomy, The University of Edinburgh, Edinburgh EH9 3FD, United Kingdom*
[2]*Theoretical Physics Department, CERN, Geneva, Switzerland*
[3]*School of Physics and Astronomy, University of Southampton, Southampton SO17 1BJ, United Kingdom*

(Received 2 August 2024; accepted 30 August 2024; published 25 September 2024)

We present the first numerical implementation of the massive symmetric-momentum-subtraction (mSMOM) renormalization scheme and use it to calculate the charm-quark mass. Based on ensembles with three flavors of dynamical domain-wall fermions with lattice spacings in the range 0.11–0.08 fm, we demonstrate that the mass scale which defines the mSMOM scheme can be chosen such that the extrapolation has significantly smaller discretization effects than the SMOM scheme. Converting our results to the $\overline{\mathrm{MS}}$ scheme we obtain $\bar{m}_c(3\ \mathrm{GeV}) = 1.008(13)$ GeV and $\bar{m}_c(\bar{m}_c) = 1.292(12)$ GeV.

DOI: 10.1103/PhysRevD.110.054512

I. INTRODUCTION

Nonperturbative massive renormalization schemes, such as the ones introduced in Ref. [1], yield renormalized correlators that satisfy vector and axial Ward identities independent of the value of the quark masses and are expected to reabsorb some of the lattice artifacts that come in powers of am and can be large for heavy-quark masses. These schemes are therefore interesting candidates to renormalize quantities that are affected by large cutoff effects, leading to milder extrapolations to the continuum limit compared to the usual massless schemes that are currently used.

In this paper, we present the first numerical implementation of the renormalization conditions that were spelled out in Ref. [1] and extract the renormalization constants that are needed in order to compute the renormalized charm-quark mass in these massive symmetric-momentum-subtraction (mSMOM) schemes. The schemes are labeled by the momentum scale of the subtraction point and by the value of the renormalized quark mass at which the renormalization conditions are imposed. Lattice artifacts depend on the choice of this mass, which can be tuned in order to obtain flatter extrapolations. We use lattice QCD ensembles generated by the RBC/UKQCD Collaboration, with $2+1$ dynamical flavors and inverse lattice spacings ranging from $a^{-1} = 1.73$ to 2.79 GeV. We compute all the lattice correlators that enter the renormalization conditions and spell out in detail the workflow to implement and solve the correct set of equations.

Results in different mSMOM schemes are converted to $\overline{\mathrm{MS}}$ using one-loop conversion factors and show a pleasing consistency. The main result of this first study confirms the theoretical expectation motivating massive schemes. They provide a (simple) way to absorb some of the mass-dependent lattice artifacts and yield more reliable extrapolations to the continuum limit.

The remainder of this paper is organized as follows. In Sec. II we remind the reader of the details of the massive nonperturbative renormalization scheme. In Sec. III we provide details of our numerical setup before presenting the details of our analysis and our final results in Sec. IV. We conclude with an outlook in Sec. V. An early stage of this analysis was reported in Ref. [2].

II. MASSIVE NONPERTURBATIVE RENORMALIZATION

Before discussing the numerical analysis that was performed for this paper, we summarize the main ideas behind massive renormalization schemes. To keep our presentation self-contained, we quote below the renormalization conditions defining mSMOM schemes, which were

*Contact author: j.t.tsang@cern.ch

originally spelled out in Ref. [1]. To match the numerical simulations, we work in Euclidean space. In our conventions, bare quantities are written without any suffix, while their renormalized counterparts are identified by a suffix R. The renormalization conditions are usually expressed in terms of amputated correlators of fermion bilinears

$$\Lambda^a_\Gamma(p_2,p_3) = S(p_3)^{-1} G^a_\Gamma(p_3,p_2) S(p_2)^{-1}, \quad (2.1)$$

where $S(p)$ is the fermion propagator,

$$S(p) = \int d^4x e^{-ip\cdot x} \langle \psi(x)\bar{\psi}(0)\rangle, \quad (2.2)$$

and $G^a_\Gamma(p_3,p_2) = \langle O^a_\Gamma(q)\bar{\psi}(p_3)\psi(p_2)\rangle$ with $O^a_\Gamma = \bar{\psi}\Gamma\tau^a\psi$. The superscript a, which will be dropped henceforth, denotes that we consider flavor nonsinglet bilinears, with τ^a a generic flavor-rotation generator. In the following we will also suppress the superscript mSMOM unless it is required to avoid ambiguity.

We choose the same symmetric-momentum configurations as those chosen in the massless SMOM [3] scheme (which is a generalization of the MOM scheme [4]), i.e., $q^2 \equiv (p_2-p_3)^2 = p_2^2 = p_3^3 = \mu^2$, where μ is the renormalization scale. The massive scheme requires the introduction of another scale $\bar{m}_R$, a renormalized mass at which the renormalization conditions are imposed. The massless scheme is recovered in the limit $\bar{m}_R \to 0$. For the mSMOM scheme in Euclidean space the renormalization conditions, to be evaluated with the symmetric-momentum configuration imposed and at $m_R = \bar{m}_R$, read

$$1 = \frac{1}{12p^2}\mathrm{Tr}[-iS_R(p)^{-1}\not{p}], \quad (2.3)$$

$$1 = \frac{1}{12m_R}\left\{\mathrm{Tr}[S_R(p)^{-1}] + \frac{1}{2}\mathrm{Tr}[(iq\cdot\Lambda_{\mathrm{A},R})\gamma_5]\right\}, \quad (2.4)$$

$$1 = \frac{1}{12q^2}\mathrm{Tr}[(q\cdot\Lambda_{\mathrm{V},R})\not{q}], \quad (2.5)$$

$$1 = \frac{1}{12q^2}\mathrm{Tr}[(q\cdot\Lambda_{\mathrm{A},R} + 2m_R\Lambda_{\mathrm{P},R})\gamma_5\not{q}], \quad (2.6)$$

$$1 = \frac{1}{12i}\mathrm{Tr}[\Lambda_{\mathrm{P},R}\gamma_5], \quad (2.7)$$

$$1 = \frac{1}{12}\mathrm{Tr}[\Lambda_{\mathrm{S},R}] + \frac{1}{6q^2}\mathrm{Tr}[2m_R\Lambda_{\mathrm{P},R}\gamma_5\not{q}]. \quad (2.8)$$

The renormalized quantities are defined as follows:

$$\psi_R = Z_q^{1/2}\psi, \qquad m_R = Z_m m, \qquad O_{\Gamma,R} = Z_\Gamma O_\Gamma, \quad (2.9)$$

where m denotes a quark mass. The renormalized propagator and amputated vertex functions are

$$S_R(p) = Z_q S(p), \quad \Lambda_{\Gamma,R}(p_2,p_3) = \frac{Z_\Gamma}{Z_q}\Lambda_\Gamma(p_2,p_3). \quad (2.10)$$

As discussed in the original publication [1], these conditions ensure that renormalized correlators satisfy the Ward identities of the continuum theory, which in turn lead to useful constraints on the renormalization constants,[1] namely

$$Z_{\mathrm{V}} = Z_{\mathrm{A}} = 1, \qquad Z_{\mathrm{P}} = Z_{\mathrm{S}}, \qquad Z_m Z_{\mathrm{P}} = 1. \quad (2.11)$$

Substituting Eqs. (2.9) and (2.10) into the renormalization conditions (2.3)–(2.8) and solving the system of equations gives access to the renormalization factors Z_q, Z_m, Z_A, Z_V, Z_S and Z_P. In practice we find it convenient to replace the renormalization condition (2.3) by a direct determination of Z_A from ratios of conserved and local axial currents. Combined with Eqs. (2.4)–(2.8) this still gives access to all the required renormalization constants.

Note that by construction the renormalization constants in a massive scheme depend on both the coupling and the dimensionless product $a\bar{m}$, where $\bar{m}$ is the bare value of the mass $\bar{m}_R$ on a given ensemble and a is the lattice spacing. The mSMOM schemes are defined by tuning the renormalized quark mass to some arbitrary scale $\bar{m}_R$, where the renormalization conditions need to be satisfied.

The arbitrariness in the choice of $\bar{m}_R$ can be turned into a useful tool when extrapolating lattice QCD results to the continuum limit. Indeed, the *ideal* choice of $\bar{m}_R$ is determined by requiring that the observables of interest have a mild dependence on the lattice spacing in that particular scheme. Different observables may dictate different values of $\bar{m}_R$; this is not a problem, since we know how to connect schemes corresponding to different choices of $\bar{m}_R$ to a common reference scheme such as, e.g., $\overline{\mathrm{MS}}$, using the one-loop perturbative expressions in Ref. [1] and in Appendix B.

The focus of this paper is to compute the renormalized charm-quark mass in mSMOM, which is defined as

$$m^{\mathrm{mSMOM}}_{c,R}(\mu,\bar{m}_R) = \lim_{a\to 0} Z^{\mathrm{mSMOM}}_m(g,a\mu,a\bar{m})(am_c)a^{-1}, \quad (2.12)$$

where the mass scale $\bar{m}_R$ defining the renormalization scheme is obtained through

$$\bar{m}_R(\mu,\bar{m}_R) = \lim_{a\to 0} Z^{\mathrm{mSMOM}}_m(g,a\mu,a\bar{m})(a\bar{m})a^{-1}, \quad (2.13)$$

[1]In [1] it was checked that the last condition in Eq. (2.8) ensured $Z_{\mathrm{S}} = Z_{\mathrm{P}}$ at one loop in continuum perturbation theory in the Feynman gauge. For other gauge choices, this condition should be modified. This renormalization condition is not used in the analysis presented in this paper.

and the bare-quark mass in lattice units (am) is the sum of the input quark mass am_q and the additive mass renormalization $am_{\rm res}$

$$am \equiv (am_q + am_{\rm res}), \tag{2.14}$$

$Z_m^{\rm mSMOM}(g, a\mu, a\bar{m})$ is the renormalization constant defined by the renormalization conditions above and the bare mass of the charm quark is set by requiring that the mass of the heavy-heavy pseudoscalar meson coincides with the mass of the physical η_c meson.

After taking the continuum limit, the mSMOM renormalized mass can be converted to $\overline{\rm MS}$,

$$m_R^{\overline{\rm MS}}(\tilde{\mu}) = R^{\overline{\rm MS}\leftarrow{\rm mSMOM}}(\tilde{\mu}, \mu, \bar{m}_R) m_R^{\rm mSMOM}(\mu, \bar{m}_R), \tag{2.15}$$

where the dimensionful scale $\tilde{\mu}$ stems from dimensional regularization and will in practice be set equal to μ. The conversion factor $R^{\overline{\rm MS}\leftarrow{\rm mSMOM}} = Z_m^{\overline{\rm MS}}/Z_m^{\rm mSMOM}$ is evaluated at one loop in perturbation theory in Appendix B.

III. SIMULATION SETUP AND STRATEGY

We use RBC/UKQCD's ensembles [5–9] with Iwasaki gauge action [10,11] and domain-wall fermion action [12,13]. They include the dynamical effects from degenerate up and down quarks as well as the strange quark. The main ensemble properties are listed in Table I. For each of the three lattice spacings we have one ensemble with the Shamir domain-wall kernel [12] (last letter "S") and one with the Möbius domain-wall kernel [14–16] (last letter "M"). The parameters of these kernels are chosen such that a combined continuum limit with all ensembles is possible [6]. In addition we have data around the physical charm-quark mass on the physical pion mass ensemble M0M which differs from M1M only in pion mass and volume.

We implement the SMOM momentum configuration by choosing momenta $p_2 = (p, p, 0, 0)$ and $p_3 = (p, 0, p, 0)$ where $p = \frac{2\pi}{L}(n + \theta)$. Since our aim is to comprehensively cover the region $2 \lesssim q \lesssim 3$ GeV we use twist angles $\theta \in \{0, 0.25, 0.5, 0.75\}$ in combination with Fourier modes $n \in \{3, 4, 5\}$ for the coarse and medium and $n \in \{4, 5, 6\}$ for the fine ensembles.

We map out the parameter space by simulating at several quark masses am_q between the light-quark mass and the largest quark mass we can reach on a given ensemble while maintaining good control over the residual-mass determination and the domain-wall formalism [17]. Since we expect sea-pion mass and finite volume effects to be negligible for the determination of the charm-quark mass, the main numerical analysis is based on the computationally cheaper nonphysical pion mass ensembles. However, in order to assess these effects, we simulated a small number of heavy-quark masses in the charm region on the M0M ensemble which can be directly compared with the equivalent M1M data points. As we will see in Sec. IV A, sea-pion mass effects are at the subpermille level.

The chosen quark masses are listed in Table II. The measurements were carried out using the Grid and Hadrons libraries [18–20].

For each input quark mass am_q we compute vertex functions [see Eq. (2.1)] as well as several mesonic flavor-diagonal quark-connected two-point correlation functions. For the latter we use a mild Jacobi smearing to improve the overlap with the ground state for heavy masses, in particular for the pseudoscalar density P, the midpoint pseudoscalar density J_{5q} [13] and the local (L) and conserved (C) [6,21,22] versions of the temporal component of the axial current. We determine the residual mass $am_{\rm res}$ and the renormalization constant Z_A from the late time behavior of ratios of these correlation functions via

$$am_{\rm res}^{\rm eff}(t) = \frac{\langle PJ_{5q}\rangle(t)}{\langle PP\rangle(t)}, \tag{3.1}$$

and

$$Z_A^{\rm eff}(t) = \frac{1}{2}\left[\frac{C(t+\frac{1}{2}) + C(t-\frac{1}{2})}{2L(t)} + \frac{2C(t+\frac{1}{2})}{L(t)+L(t+1)}\right]. \tag{3.2}$$

Throughout this work we set the quark mass using the quark-connected flavor-diagonal pseudoscalar meson M_{η_h},

TABLE I. Summary of the main parameters of the ensembles used in this work. In the ensemble name the first letter (C, M or F) stands for coarse, medium and fine, respectively. The last letter (M or S) stands for Möbius and Shamir kernels, respectively.

Name	L/a	T/a	a^{-1} (GeV)	M_π (MeV)	am_l	am_s
C1M	24	64	1.7295(38)	276	0.005	0.0362
C1S	24	64	1.7848(50)	340	0.005	0.04
M0M	64	128	2.3586(70)	139	0.000678	0.02661
M1M	32	64	2.3586(70)	286	0.004	0.02661
M1S	32	64	2.3833(86)	304	0.004	0.03
F1M	48	96	2.708(10)	232	0.002144	0.02144
F1S	48	96	2.785(11)	267	0.002144	0.02144

TABLE II. Heavier input quark masses that were simulated in addition to am_l, $2am_l$, $am_s/2$ and am_s.

Ensemble	am_q
C1M	0.05, 0.1, 0.15, 0.2, 0.3
C1S	0.05, 0.1, 0.15, 0.2, 0.3, 0.33
M1M	0.05, 0.1, 0.15, 0.225, 0.3, 0.32, 0.34
M1S	0.05, 0.1, 0.15, 0.225, 0.3, 0.32, 0.34, 0.36, 0.375
F1M	0.033, 0.066, 0.099, 0.132, 0.198, 0.264, 0.33, 0.36
F1S	0.033, 0.066, 0.099, 0.132, 0.198, 0.264, 0.33, 0.36, 0.396

since the quantity we are ultimately interested in is the charm-quark mass and the contribution from quark-disconnected pieces to the mass of the η_c meson has been estimated to be negligibly small [23]. We explore reference masses in the range $\frac{1}{2}M_{\eta_c}^{\mathrm{PDG}}$–$M_{\eta_c}^{\mathrm{PDG}} = 2.9839(4)$ GeV [24].

The strategy of our calculation is as follows:

(a) For each mass am_q on each ensemble, determine am_{res} and hence am as well as $aM_{\eta_h}(am)$, $Z_A(g, am)$, $Z_m(g, a\mu, am)$.

(b) Interpolate $Z_m(g, a\mu, am)$ to a common momentum scale $\hat{\mu}$ to obtain $Z_m(g, a\hat{\mu}, am)$ on all ensembles.

(c) Fix two mass scales: the scale $\bar{m}$ at which the renormalization conditions are imposed and the quark mass m to be determined. These do not have to be the same.

In practice we define a set of meson masses M_i such that $M_i/M_{\eta_c}^{\mathrm{PDG}} \in \{0.5, 0.6, 0.7, 0.75, 0.8, 0.9, 1\}$. We interpolate $am(aM)$ to each choice of M_i to obtain am_i and similarly interpolate $Z_m(g, a\hat{\mu}, am)$ to obtain $Z_m(g, a\hat{\mu}, am_i)$. We note that the heaviest two and three values of M_i are not directly accessible on the C1S and C1M ensembles, respectively.

Then, we define the mass scale $\bar{m}$ of the renormalization condition by fixing a meson mass $\bar{M}$ to be one of the M_i and set the bare-quark mass m by fixing a meson mass M to a potentially different M_i.

(d) For the given choice of M and $\bar{M}$, combine $Z_m(g, a\hat{\mu}, a\bar{m})$ and am to obtain the right-hand side of Eq. (2.12) on each ensemble. Take the continuum limit to obtain $m_R(\hat{\mu}, \bar{m}_R)$. Finally (since M and $\bar{M}$ can differ), also take the continuum limit to obtain $\bar{m}_R(\hat{\mu}, \bar{m}_R)$ [cf. Eq. (2.13)]. This last step is required in order to know the mass scale of the renormalization condition which is needed to relate it to other schemes such as SMOM or $\overline{\mathrm{MS}}$.

(e) Our choice of domain-wall parameters does not allow for direct simulations at the physical charm-quark mass on the coarse lattice spacing. Hence we repeat this procedure for different values of M, but at fixed $\bar{M}$. This yields values $m_{i,R}^{\mathrm{mSMOM}}(\hat{\mu}, \bar{m}_R)$ as a function of M_i, which can be parametrized to finally obtain the value of $m_{c,R}^{\mathrm{mSMOM}}(\hat{\mu}, \bar{m}_R)$.

(f) Finally, repeat the entire analysis for different choices of $\hat{\mu}$ and $\bar{M}$ in order to determine the *ideal* choice of $\bar{m}$ for a given $\hat{\mu}$.

IV. RESULTS

In this section we carry out the analysis outlined above.

A. From correlators to observables

We first determine am_{res}, Z_A and aM on all ensembles and for each choice of quark mass. The plots in Fig. 1 illustrate the time behavior of the data on the M1M ensemble [cf. Eqs. (3.1) and (3.2)] from which these quantities can be determined at late times. As expected

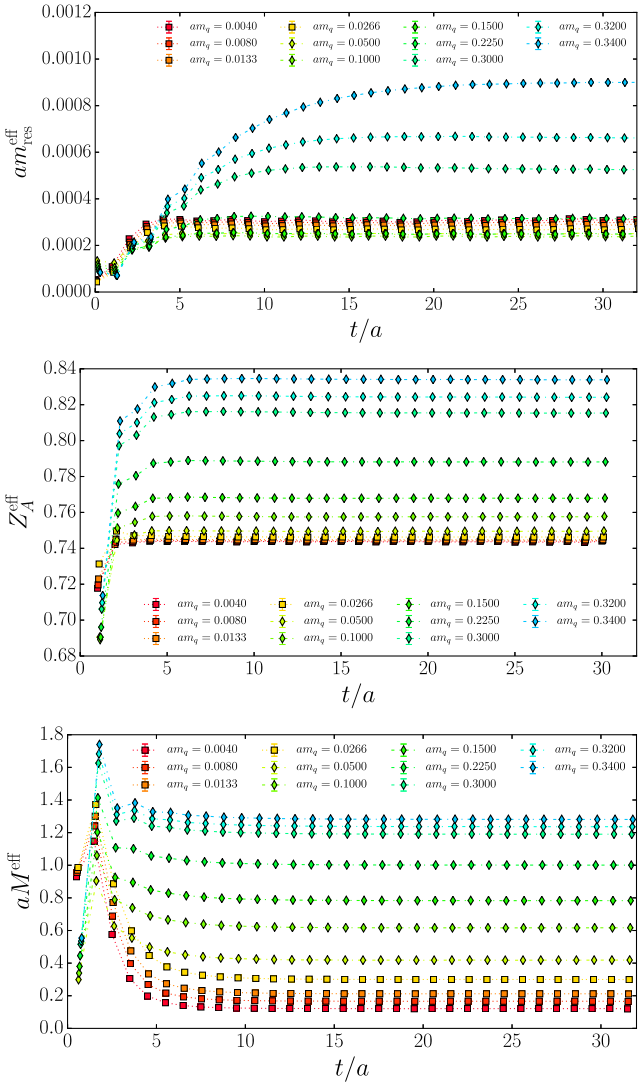

FIG. 1. Representative effective am_{res} (top) and Z_A (middle) and aM_{η_h} (bottom) values on the M1M ensemble.

from our previous work [17], we find that, for large quark masses, the residual mass grows and eventually becomes unbounded. We conservatively discard any data where this might be the case and only show data points for which the residual mass reaches a plateau at late times. We observe stable plateaus for all data points that are included in the analysis. Since the data are very precise and the plateaus are unambiguous, we do not perform fits to the data, but simply take the midpoint value (rightmost points in the plots in Fig. 1). Numerical values for all data points are presented in Tables V–X in Appendix A. Figure 3 shows the spectrum as a function of the bare-quark mass m. Combining the determination of Z_A for each simulated mass point with the system of equations (2.4)–(2.8) we obtain the corresponding values of Z_m^{mSMOM} at each mass point for the simulated renormalization scales μ.

Before performing the required interpolations and continuum extrapolations, we consider the size of potential

TABLE III. Comparison of observables between the M0M ($M_\pi = 139$ MeV) and the M1M ($M_\pi = 286$ MeV) ensembles for two mass points bracketing the physical charm-quark mass.

0.32	M0M	M1M	M0M/M1M
aM	1.23636(19)	1.23593(61)	1.00035(53)
am_{res}	0.0006613(18)	0.0006617(21)	0.9993(41)
Z_A	0.824110(43)	0.824154(95)	0.99995(12)
0.34	**M0M**	**M1M**	**M0M/M1M**
aM	1.28092(18)	1.28049(61)	1.00033(50)
am_{res}	0.0009049(26)	0.0009004(28)	1.0050(43)
Z_A	0.833863(42)	0.833897(100)	0.99996(13)

effects afflicting simulations which do not take place at the physical pion mass. Table III contrasts the values for aM, am_{res} and Z_A on the M0M and the M1M ensembles for two choices of the heavy-quark mass that bracket the physical charm-quark mass. These two ensembles only differ in their volume and pion mass. We observe that the respective values on M0M and M1M are compatible with each other and hence their ratios are compatible with unity. We further observe that the relative (albeit not statistically resolved) effect on the hadron mass is at the subpermille level. We therefore conclude that any chiral effects in the data can be safely neglected.

B. Interpolations

Having obtained $Z_m^{\text{mSMOM}}(g, a\mu, am)$, $M(am)$ and am at each simulated mass point, we now perform the interpolations listed in steps (b) and (c). Given the broad range covered by our data (cf. Figs. 2 and 3), we perform these interpolations locally as polynomial fits to the closest data points. In order to estimate any systematic uncertainties stemming from these interpolations we perform them in multiple ways:

(i) linear interpolation between the two closest bracketing data points;

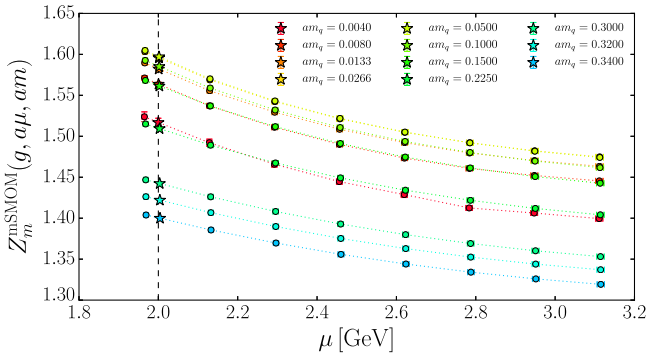

FIG. 2. Interpolation of Z_m to a scale of $\mu = 2$ GeV for various input quark mass am_q on the M1M ensemble. The stars indicate the value of Z_m^{mSMOM} interpolated to $\hat{\mu} = 2$ GeV.

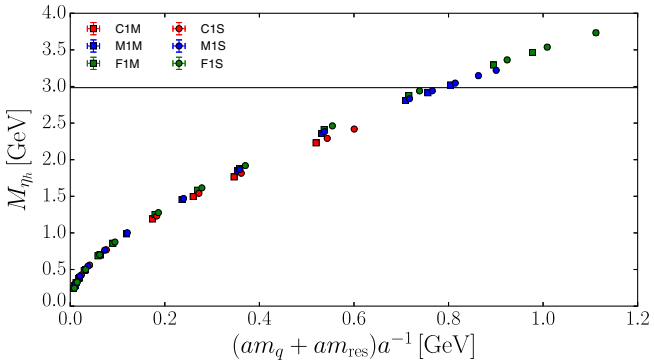

FIG. 3. Coverage of the quark mass dependence of our data.

(ii) quadratic interpolations between the two data points which bracket the target value and the nearest other data point to the left (right);

(iii) a cubic interpolation between the closest four points.

We take the quadratic interpolation with the third data point closest to the target value as our central value and in addition to its statistical uncertainty assign half the spread between these values as a systematic uncertainty. Figure 2 illustrates this for step (b), i.e., the interpolation of Z_m at fixed mass ($am_q = 0.15$) to the scale of $\mu = 2$ GeV. Since we want to contrast the approach to the continuum limit between the massless (SMOM) and the massive (mSMOM) scheme, we also compute Z_m^{SMOM}.

For completeness, we list the numerical values for Z_m^{mSMOM} and Z_m^{SMOM} at $\mu = 2$ GeV in Tables V–X. We compute Z_m^{SMOM} only in the light and strange sector and use these values to extrapolate Z_m^{SMOM} to the massless limit, prior to applying it.

C. Continuum extrapolations

Having determined am, $a\bar{m}$ and $Z_m(g, a\hat{\mu}, a\bar{m})$ on each ensemble, we can now perform the continuum limit of the renormalized quark mass am using the mSMOM scheme at a renormalization scale $\hat{\mu}$ and mass scale $\bar{m}$. The most general ansatz that we consider for our continuum extrapolations is given by

$$m(a\Lambda, a\hat{\mu}) = m(\hat{\mu}) + C_\chi am_{\text{res}} + C_1(a\Lambda)^2, \quad (4.1)$$

where the coefficient C_χ captures scaling violations stemming from the residual chiral symmetry breaking in our data. We tried adding a term proportional to a^4 but in practice we find that the term proportional to a^4 is compatible with zero and not needed to describe the data and we hence do not include it in the ansatz. Contrary to this, the coefficient C_χ is typically resolved from zero and tends to be of $O(1)$. However, the size of am_{res} is typically small (cf. Tables V–X).

We present an example continuum limit fit in the top panel of Fig. 4 for the choice $\bar{M} = 0.7 \times M_{\eta_c}^{\text{PDG}}$ and

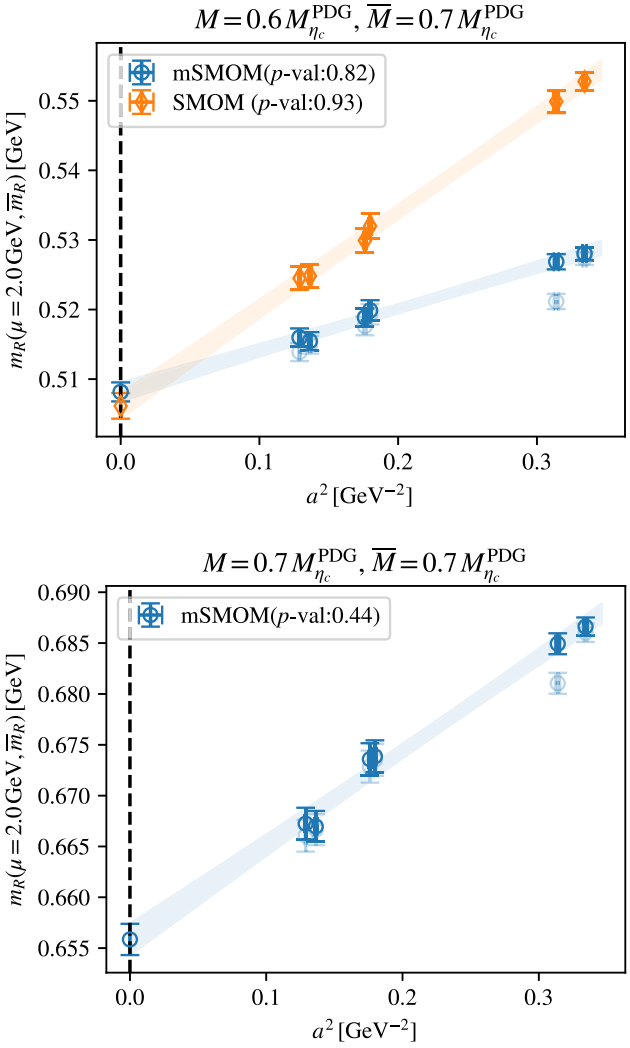

FIG. 4. Top: example continuum limit extrapolation comparing the approach to the continuum for the SMOM scheme to the that of the mSMOM scheme. The quark masses m_R (that is being extrapolated) and $\bar{m}_R$ (defining the mSMOM scheme) are chosen to reproduce mesons of mass $0.6 \times M_{\eta_c}^{\rm PDG}$ and $0.7 \times M_{\eta_c}^{\rm PDG}$, respectively. Bottom: continuum limit determining the renormalization mass scale $\bar{m}_R$ at which the renormalization conditions are imposed.

$M = 0.6 \times M_{\eta_c}^{\rm PDG}$. In addition to the mSMOM data points (blue circles) we also show the approach to the continuum limit using the chirally extrapolated value of Z_m in the SMOM scheme (orange diamonds). We clearly see that the data have smaller discretization effects in the mSMOM scheme than the SMOM scheme. The continuum extrapolated values are not expected to agree with each other, since they are not converted to the same scheme yet. However, when evaluating the conversion factors for the scale and mass at hand (compare the right-hand panel of Fig. 10 in Appendix B), we find the conversion factor to be very close to unity. In order to determine the exact parameters of the scheme it remains to determine the value of $\bar{m}$, i.e., to take

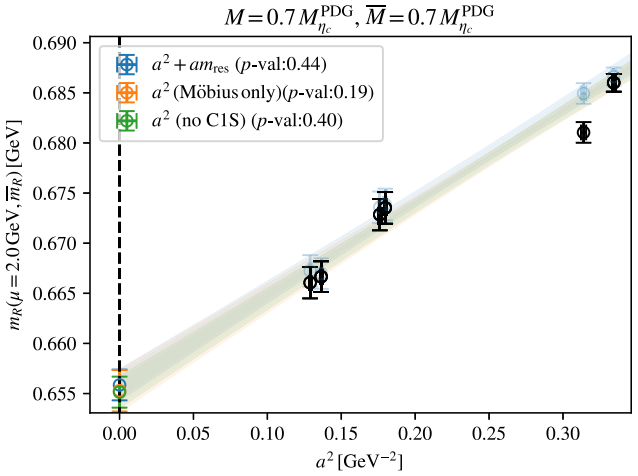

FIG. 5. Variations of the continuum limit extrapolation presented in the bottom panel of Fig. 4.

the continuum limit where $M = \bar{M}$. This is shown for the value $0.7 \times M_{\eta_c}^{\rm PDG}$ in the bottom panel of Fig. 4.

In both plots, the original mSMOM data points are shown as partially transparent blue symbols; the opaque blue symbols present the value once the residual-mass contribution is corrected for. We notice that this only significantly affects the C1S data point, which is expected since residual chiral symmetry breaking effects are known to decrease as the lattice spacing is reduced and when increasing the Möbius scale which is one for the Shamir kernel and two for the Möbius kernel we are using.[2] In addition, the residual mass is known to increase as the input quark mass am_q increases as can be seen, e.g., in the top panel of Fig. 1.

In order to assess the systematic uncertainties associated with the continuum limit extrapolation we repeat the fit for several variations. In particular Fig. 5 shows this for the case of the combination of masses $(M, \bar{M})$ presented in the top panel of Fig. 4. We consider

(i) fitting all ensembles on which the hadron mass M can be simulated including the terms proportional to $am_{\rm res}$ and $(a\Lambda)^2$;
(ii) fitting all except the C1S ensemble (which has by far the largest $am_{\rm res}$ value) only including the term proportional to $(a\Lambda)^2$;
(iii) fitting only the Möbius ensembles (which have smaller $am_{\rm res}$ values) only including the term proportional to $(a\Lambda)^2$.

We quote the first of these fits as our central value and additionally assign half the spread of the variations as a systematic uncertainty from the choice of continuum limit.

[2]The residual chiral symmetry breaking of our choice of Möbius kernel is expected to be the same as that of the Shamir kernel with twice the extent of the fifth dimension L_s. Since $L_s(C1S) = 16$ and $L_s(C1M) = 24$ the C1M ensemble effectively has a 3 times larger extent of the fifth dimension.

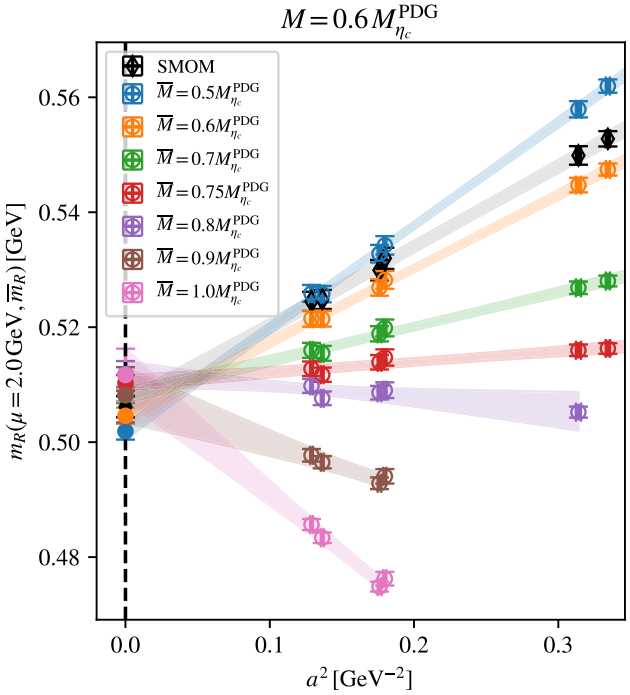

FIG. 6. Variations of the renormalization mass scale $\bar{M}$ at fixed value of M. The data are fitted to Eq. (4.1) and the plot displays it after correcting to vanishing residual mass. The black data points show the approach to the continuum for the case of the massless SMOM scheme. We stress that different values of $\bar{m}$ define different schemes, hence these numbers are *not* expected to agree in the continuum limit.

D. Varying the renormalization scales

We stress that the renormalization mass scale $\bar{m}_R$ set by $\bar{M}$ is a scale that can be varied freely within the range where we have data. In Fig. 6 we presents fits to the ansatz (4.1) $M = 0.6 \times M_{\eta_c}^{\mathrm{PDG}}$ but for a variety of choices of $\bar{M}$. We emphasize again that the extrapolated values do not have to agree as they are still in different schemes. It is however clearly visible that the approach to the continuum is well described by a fit linear in a^2 but that the slope varies strongly with the choice of $\bar{M}$. For the largest values of $\bar{M}$ we lose coverage on the coarsest ensembles and hence remove them from the fit. For the remaining analysis we restrict ourselves to values of $\bar{M}$ that allow direct simulations on all considered ensembles.

We also vary the renormalization scale μ between 2.0, 2.5 and 3.0 GeV. We observe that for increasing values of μ the values of $\bar{M}$ which are required to significantly flatten the continuum limit are beyond the range where we can determine $\bar{m}$ from all three lattice spacings. We therefore base our final results on continuum limit extrapolations at $\mu = 2$ GeV and only show the corresponding mSMOM results obtained from larger scales for comparison (cf. Table IV).

E. The charm-quark mass

We now vary the choice of M using the various M_i and repeat the continuum limit fit for each case, keeping $\bar{M}$ fixed in order to remain in the same scheme. For each choice M_i we assemble the error budget of this fit to obtain values $m_i^{\mathrm{mSMOM}}(2\ \mathrm{GeV}, \bar{m})$. We now combine these results to perform an inter- or extrapolation to the physical charm-quark mass. This is not strictly speaking necessary, since we already have a direct result for this quark mass from the continuum limit at $M_i = M_{\eta_c}^{\mathrm{PDG}}$, however since this continuum limit is only based on the medium and fine ensembles we prefer to supplement it by a parametrization using different values (in the continuum) of m_i^R/M_i as a function of M_i. This is shown in Fig. 7. Of our choices for M_i we consider the ranges $M_i/M_{\eta_c}^{\mathrm{PDG}}$ [0.6, 1.0], [0.7, 1.0], [0.6, 0.9] and [0.6, 0.8]. In each case we parametrize the dependence of the quark mass as a polynomial in M_i via

TABLE IV. Summary of our final results for the charm-quark mass. We quote the renormalization mass scale $\bar{m}_R^{\mathrm{mSMOM}}$ defining the given mSMOM scheme, as well as the charm-quark mass in that scheme, converted to $\overline{\mathrm{MS}}$ at the same scale and to $\overline{\mathrm{MS}}$ at $\bar{m}_c$. For comparison we also quote the results obtained from the SMOM renormalization conditions. All quark masses are given in units of GeV.

μ/GeV	$\bar{M}/M_{\eta_c}^{\mathrm{PDG}}$	$\bar{m}_R(\mu, \bar{m}_R)$	$m_{c,R}^{\mathrm{RI}}(\mu, \bar{m}_R)$	$\bar{m}_c^{\overline{\mathrm{MS}}}(\mu)$	$\bar{m}_c^{\overline{\mathrm{MS}}}(3\ \mathrm{GeV} \leftarrow \mu)$	$\bar{m}_c^{\overline{\mathrm{MS}}}(\bar{m}_c)$
2.0	0.60	0.5046(15)	1.127(7)(12)	1.112(7)(12)(4)	1.005(6)(11)(4)	1.289(6)(10)(3)
2.0	0.70	0.6559(16)	1.129(7)(12)	1.115(7)(12)(4)	1.008(6)(11)(4)	1.292(5)(10)(4)
2.0	0.75	0.7371(16)	1.130(6)(13)	1.118(6)(13)(4)	1.010(6)(11)(4)	1.294(5)(10)(4)
2.0	SMOM	⋯	1.136(9)(12)	1.114(9)(12)	1.007(8)(10)	1.291(8)(10)
2.5	0.60	0.4698(14)	1.052(7)(14)	1.038(7)(14)(3)	0.995(7)(14)(3)	1.280(6)(13)(3)
2.5	0.70	0.6124(16)	1.057(6)(15)	1.043(6)(15)(3)	1.000(6)(14)(3)	1.284(6)(13)(3)
2.5	0.75	0.6894(16)	1.059(6)(15)	1.046(6)(15)(3)	1.003(6)(15)(3)	1.287(5)(13)(3)
2.5	SMOM	⋯	1.066(11)(12)	1.048(10)(12)	1.004(10)(12)	1.288(9)(11)
3.0	0.60	0.4450(14)	0.998(7)(15)	0.986(7)(15)(3)	0.986(7)(15)(3)	1.271(6)(14)(2)
3.0	0.70	0.5811(15)	1.004(6)(15)	0.992(6)(15)(3)	0.992(6)(15)(3)	1.277(5)(14)(2)
3.0	0.75	0.6549(16)	1.008(6)(16)	0.995(6)(16)(3)	0.995(6)(16)(3)	1.280(5)(15)(2)
3.0	SMOM	⋯	1.018(8)(12)	1.002(8)(12)	1.002(8)(12)	1.287(8)(11)

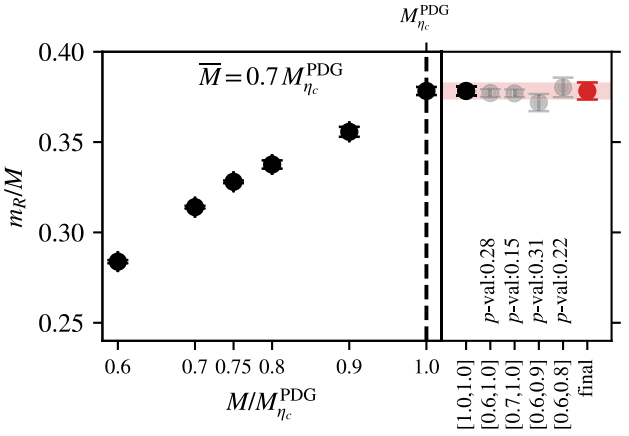

FIG. 7. Extrapolation of different intervals of the various reference values M to the physical value $M_{\eta_c}^{\rm PDG}$ at fixed $\bar{M}$. The right side shows results for these interval choices. The red data point to the very right and the corresponding band represents our final value of $m_{c,R}$ in the mSMOM scheme at $\bar{M} = 0.7 M_{\eta_c}^{\rm PDG}$.

$$\frac{m_R}{M} = \alpha M^{-1} + \beta + \gamma M. \tag{4.2}$$

The result to these variations is shown in the right-hand panel of Fig. 7. We take the direct determination at the charm quark mass (i.e., $M_i = M_{\eta_c}^{\rm PDG}$) as central value and in addition to its uncertainty we conservatively associate a systematic uncertainty of half the spread of the variation. These fit results that determine this uncertainty are shown on the right-hand side of Fig. 7. We quote the two uncertainties separately, since the latter only arises since we require our final number to be based on continuum limits from more than two lattice spacings. With additional finer ensembles, this last uncertainty would be completely removed, since a continuum limit with three lattice spacings could be obtained directly at the charm-quark mass. We then repeat the analysis for different choices of $\bar{M}$ (and hence $\bar{m}_R$) as well as the massless SMOM scheme.

Finally, it remains to convert these results into a common scheme where they can be directly compared to each other. Using the conversion factor $R_m^{\overline{\rm MS}\leftarrow{\rm mSMOM}}$ given in Eq. (B18), we can convert the results from $m_{c,R}^{\rm mSMOM}(\mu, \bar{m}_R)$ to $m_{c,R}^{\overline{\rm MS}}(\mu)$. Unfortunately, for the mSMOM scheme, this is currently only known at one loop. In order to quantify the truncation effects in the temporary absence of perturbative two-loop calculations, we investigate the difference between one- and two-loop corrections for the massless scheme [25,26] and assign the relative difference between them as a systematic truncation uncertainty. In practice we find that for $\mu = 2.0$ GeV (2.5, 3.0 GeV) the difference between one- and two-loop conversion to $\overline{\rm MS}$ is a 0.38% (0.31%, 0.27%) effect. Within the $\overline{\rm MS}$ scheme we then run the results up to 3 GeV as well as down to the charm-quark scale to quote $\bar{m}_c(\bar{m}_c)$. To compute the strong coupling and running of the $\overline{\rm MS}$ quark mass we make use of RunDec [27–29], which in turn relies on five-loop results for the β function and for the mass anomalous dimension [30–35].

We list these results for some choices of $\bar{M}$ and μ in Table IV where the first uncertainty is the result from the pure mSMOM calculation at a chosen quark mass, the second uncertainty list encapsulates the charm-mass interpolation, and the last uncertainty estimates the truncation effect due to performing the matching at one loop. In principle one could also quote a fourth uncertainty encapsulating the uncertainties of the inputs to the running and the truncation of the running factor, however these are found to be negligible.

Our final results for the charm-quark mass converted to $\overline{\rm MS}$ and then (where necessary) run to 3 GeV within the $\overline{\rm MS}$ scheme are shown in Fig. 8. As mentioned above, in the massive scheme the continuum limit is well controlled for determinations at $\mu = 2$ but values of $\bar{M}$ which significantly decrease the slope of the continuum limit are not reachable on our current dataset for larger values of μ and we therefore exclude them. We find good agreement between the SMOM and the mSMOM schemes as well as among different values for $\bar{m}_R$ within the mSMOM scheme. As our final number we quote our results obtained from mSMOM at $\hat{\mu} = 2$ GeV from the choice $\bar{M} = 0.7 M_{\eta_c}^{\rm PDG}$ which corresponds to $\bar{m}_R^{\rm mSMOM} = 0.6559(16)$ GeV. We find

$$m_{c,R}^{\rm mSMOM}(2\ {\rm GeV}, \bar{m}_R) = 1.129(7)(12)\ {\rm GeV}, \tag{4.3}$$

$$m_{c,R}^{\overline{\rm MS}}(2\ {\rm GeV}) = 1.115(7)(12)(4)\ {\rm GeV}, \tag{4.4}$$

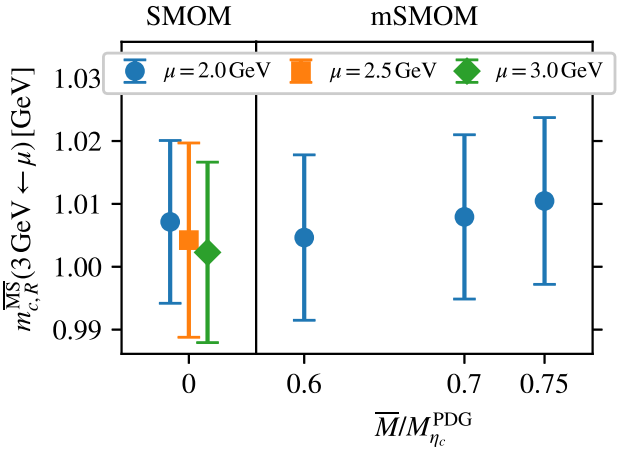

FIG. 8. Results for the continuum-extrapolated renormalized charm-quark mass converted to $\overline{\rm MS}$ from regularization invariant RI/SMOM and RI/mSMOM with variation in $\bar{M}$ at renormalization scale of 3 GeV using results from $\mu = 2.0, 2.5, 3.0$ GeV. Numerical values are presented in Table IV.

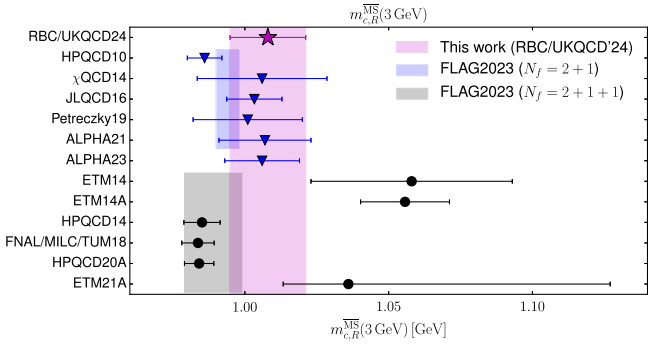

FIG. 9. Comparison of our result with previous determinations of the charm quark mass in the literature that enter the FLAG [36] average. The magenta star and corresponding band are our result, the blue triangles are results based on $N_f = 2+1$ [37–41] and the black circles based on $N_f = 2+1+1$ [42–47]. The blue and black bands show the corresponding FLAG averages for $N_f = 2+1$ and $N_f = 2+1+1$, respectively. In addition we display the recent ALPHA23 determination [48] which has appeared since the last FLAG review.

$$m_{c,R}^{\overline{\rm MS}}(3\ {\rm GeV}) = 1.008(6)(11)(4)\ {\rm GeV}, \tag{4.5}$$

$$m_{c,R}^{\overline{\rm MS}}(m_{c,R}^{\overline{\rm MS}}) = 1.292(5)(10)(4)\ {\rm GeV}, \tag{4.6}$$

$$m_{c,R}^{\overline{\rm MS}}(1.292\ {\rm GeV}) = 1.292(7)(14)(6)\ {\rm GeV}. \tag{4.7}$$

The first uncertainty comes from the determination directly at the charm-quark mass, the second from the inter-/extrapolation taking smaller than physical reference values, and the third from the perturbative truncation uncertainty when converting to $\overline{\rm MS}$. In Eq. (4.6) we give the $\overline{\rm MS}$ charm-quark mass evaluated at its own scale, that is, the μ for which $m_{c,R}^{\overline{\rm MS}}(\mu) = \mu$, starting from the $\overline{\rm MS}$ charm-quark mass, with error, at the fixed scale 2 GeV in (4.4). Since this mass and scale are identical, with identical uncertainties, we also give, in Eq. (4.7), the $\overline{\rm MS}$ charm-quark mass run to the fixed scale 1.292 GeV. We have not applied any additional uncertainties associated with the running within $\overline{\rm MS}$.

F. Comparison to the literature

The charm-quark mass has been previously computed by various collaborations in various schemes. In Fig. 9 we compare our result to the results in the literature which enter the FLAG average in the $\overline{\rm MS}$ scheme at 3 GeV.[3] We find good agreement with other $N_f = 2+1$ calculations and obtain similar uncertainties. The leading uncertainty in our calculation arises from the fact that not all the ensembles we currently use allow for direct simulation at the physical charm-quark mass. Using an additional finer lattice spacing will allow one to eliminate this uncertainty in the future.

[3]In cases where the results were quoted at 2 GeV, we follow FLAG's convention and apply a running factor of 0.900 to obtain the result at 3 GeV.

V. SUMMARY AND OUTLOOK

We have presented the first numerical implementation of the massive nonperturbative renormalization scheme which was first suggested in Ref. [1]. We find that varying the mass scale at which the renormalization conditions are imposed can be used to significantly modify the approach to the continuum limit and in particular to flatten it. We observe good agreement between different renormalization mass scales (and hence continuum limit approaches), further substantiating that the continuum limit is controlled.

This scheme can be applied to any observable and hence can be used to provide more reliable continuum limits. A nontrivial test is that the continuum results obtained with different choices of the renormalization mass scale should agree once converted to a common renormalization scheme, such as $\overline{\rm MS}$. This idea should be useful for any observable with large discretization effects compared to the desired statistical precision.

The joint continuum limit fits to the chosen Möbius and Shamir domain-wall kernels with very similar lattice spacings agree well with only fitting the Möbius ensembles and (at the present level of precision) are well described by an ansatz that is linear in a^2. We obtain the charm-quark mass in the $\overline{\rm MS}$ scheme at 3 GeV with a precision of 1.3% in good agreement with the literature. This uncertainty can be significantly reduced by using additional finer ensembles. By direct computation, we find the sea-pion effect on the charmed meson mass M_{η_c} between a pion mass of 286 MeV and the physical pion mass to be below the permille level.

For the future, we envisage applications of the mSMOM scheme to other observables and an extension to four quark operators.

ACKNOWLEDGMENTS

We thank our colleagues in the RBC and UKQCD Collaborations for many fruitful discussions. We are particularly grateful to Peter Boyle for valuable discussions and maintaining the Grid software package. We thank Chris Sachrajda and Matteo Di Carlo for helpful theoretical discussions in the early stages of this work. We thank Antonin Portelli for maintaining the Hadrons package. L. D. D. is funded by the UK Science and Technology Facility Council (STFC) Grant No. ST/P000630/1 and by the ExaTEPP project EP/X01696X/1. F. E. has received funding from the European Union's Horizon Europe research and innovation program under the Marie Skłodowska-Curie Grant Agreement No. 101106913. R. M. is funded by a University of Southampton Presidential Scholarship. This work used the DiRAC Extreme Scaling service at the University of Edinburgh, operated by the Edinburgh

Parallel Computing Centre on behalf of the STFC DiRAC HPC Facility. This equipment was funded by BIS National E-infrastructure capital Grant No. ST/K000411/1, STFC capital Grant No. ST/H008845/1, and STFC DiRAC Operations Grants No. ST/K005804/1 and No. ST/K005790/1.

APPENDIX A: NUMERICAL RESULTS

In Tables V–X we summarize the numerical data for the residual mass Z_A and the hadron mass aM as well as the renormalization constant Z_m interpolated to a scale of 2 GeV.

TABLE V. Summary of numerical results on the C1M ensemble used for the analysis. The values of Z_m are given after interpolation to $\mu = 2$ GeV.

C1M	$10^3 am_{\mathrm{res}}$	aM	Z_A	Z_m^{mSMOM}	Z_m^{SMOM}
0.0050	0.601(12)	0.1642(34)	0.71302(34)	1.5754(65)	1.5428(15)
0.0100	0.574(11)	0.2203(22)	0.71337(19)	1.6088(36)	1.5442(12)
0.0181	0.5330(95)	0.2886(14)	0.71443(12)	1.6211(22)	1.5425(11)
0.0362	0.4642(79)	0.40331(87)	0.717257(77)	1.6232(15)	1.5362(10)
0.0500	0.450(17)	0.4769(22)	0.71979(19)	1.6185(14)	⋯
0.1000	0.361(12)	0.6877(14)	0.72921(11)	1.5996(12)	⋯
0.1500	0.3210(100)	0.8637(11)	0.74087(11)	1.5725(10)	⋯
0.2000	0.3172(94)	1.01971(85)	0.75528(13)	1.53813(93)	⋯
0.3000	0.599(16)	1.28930(50)	0.79647(16)	1.44377(74)	⋯

TABLE VI. Summary of numerical results on the C1S ensemble used for the analysis. The values of Z_m are given after interpolation to $\mu = 2$ GeV.

C1S	$10^3 am_{\mathrm{res}}$	aM	Z_A	Z_m^{mSMOM}	Z_m^{SMOM}
0.0050	3.162(19)	0.1885(29)	0.71796(44)	1.3145(75)	1.5410(19)
0.0100	3.085(18)	0.2367(21)	0.71822(28)	1.4381(35)	1.5411(14)
0.0200	2.938(16)	0.3129(15)	0.71942(17)	1.5245(18)	1.5392(12)
0.0400	2.720(12)	0.4304(10)	0.72235(12)	1.5706(12)	1.5325(12)
0.0500	2.644(22)	0.4829(18)	0.72413(27)	1.5772(14)	⋯
0.1000	2.427(15)	0.6904(14)	0.73344(23)	1.5763(12)	⋯
0.1500	2.420(11)	0.8636(11)	0.74507(19)	1.5542(11)	⋯
0.2000	2.6192(92)	1.01733(94)	0.75960(15)	1.5210(10)	⋯
0.3000	4.530(18)	1.28409(79)	0.80194(14)	1.42069(78)	⋯
0.3300	6.455(18)	1.35527(38)	0.821474(90)	1.37464(67)	⋯

TABLE VII. Summary of numerical results on the M1M ensemble used for the analysis. The values of Z_m are given after interpolation to $\mu = 2$ GeV.

M1M	$10^3 am_{\mathrm{res}}$	aM	Z_A	Z_m^{mSMOM}	Z_m^{SMOM}
0.0040	0.3116(61)	0.1196(26)	0.74376(24)	1.5167(51)	1.5743(21)
0.0080	0.3018(56)	0.1651(16)	0.74421(13)	1.5635(26)	1.5722(23)
0.0133	0.2907(51)	0.2113(12)	0.744798(86)	1.5820(20)	1.5709(20)
0.0266	0.2709(39)	0.29939(79)	0.746330(56)	1.5955(18)	1.5667(18)
0.0500	0.2527(54)	0.4178(17)	0.749495(88)	1.5970(16)	⋯
0.1000	0.2414(40)	0.6163(11)	0.757548(60)	1.5851(15)	⋯
0.1500	0.2523(35)	0.78311(79)	0.767843(47)	1.5612(14)	⋯
0.2250	0.3173(27)	1.00082(63)	0.788084(41)	1.5093(11)	⋯
0.3000	0.5277(20)	1.19017(57)	0.815321(43)	1.44227(90)	⋯
0.3200	0.6634(21)	1.23610(64)	0.824062(46)	1.42193(84)	⋯
0.3400	0.8998(26)	1.28063(63)	0.833810(56)	1.39986(79)	⋯

TABLE VIII. Summary of numerical results on the M1S ensemble used for the analysis. The values of Z_m are given after interpolation to $\mu = 2$ GeV.

M1S	$10^3 am_{\mathrm{res}}$	aM	Z_A	Z_m^{mSMOM}	Z_m^{SMOM}
0.0040	0.6727(72)	0.1290(24)	0.74486(27)	1.5055(58)	1.5720(26)
0.0080	0.6561(64)	0.1714(16)	0.74542(15)	1.5557(28)	1.5708(21)
0.0150	0.6319(55)	0.2283(11)	0.746212(91)	1.5802(19)	1.5690(19)
0.0300	0.5977(42)	0.32118(69)	0.747987(58)	1.5930(18)	1.5639(18)
0.0500	0.5767(52)	0.42023(76)	0.75062(11)	1.5951(18)	⋯
0.1000	0.5479(35)	0.61780(44)	0.758721(100)	1.5838(17)	⋯
0.1500	0.5602(29)	0.78382(43)	0.769158(89)	1.5596(15)	⋯
0.2250	0.6677(29)	1.00056(52)	0.789767(76)	1.5066(13)	⋯
0.3000	1.0409(41)	1.18880(56)	0.817587(74)	1.43775(99)	⋯
0.3200	1.2562(65)	1.23385(41)	0.826456(79)	1.41695(97)	⋯
0.3400	1.6053(82)	1.27801(40)	0.836317(81)	1.39437(87)	⋯
0.3600	2.189(11)	1.32043(39)	0.847392(85)	1.36951(81)	⋯
0.3750	2.936(12)	1.35187(55)	0.857047(90)	1.34809(77)	⋯

TABLE IX. Summary of numerical results on the F1M ensemble used for the analysis. The values of Z_m are given after interpolation to $\mu = 2$ GeV.

F1M	$10^3 am_{\mathrm{res}}$	aM	Z_A	Z_m^{mSMOM}	Z_m^{SMOM}
0.0021	0.2399(56)	0.0865(21)	0.75927(21)	1.4816(57)	1.5797(23)
0.0043	0.2390(52)	0.1172(16)	0.75952(11)	1.5229(31)	1.5802(21)
0.0107	0.2343(43)	0.1795(10)	0.760226(53)	1.5766(21)	1.5792(19)
0.0214	0.2286(36)	0.25287(54)	0.761281(42)	1.5924(20)	1.5759(18)
0.0330	0.2244(31)	0.31620(38)	0.762536(41)	1.5942(19)	⋯
0.0660	0.2201(21)	0.46183(32)	0.766829(40)	1.5935(19)	⋯
0.0990	0.2248(15)	0.58391(32)	0.772132(39)	1.5838(18)	⋯
0.1320	0.2378(12)	0.69368(30)	0.778456(38)	1.5683(16)	⋯
0.1980	0.29064(77)	0.88979(25)	0.794371(35)	1.5243(14)	⋯
0.2640	0.39970(57)	1.06271(21)	0.815121(32)	1.4682(11)	⋯
0.3300	0.66808(62)	1.21606(19)	0.841614(31)	1.40308(87)	⋯
0.3600	1.0280(12)	1.27967(19)	0.856367(32)	1.36962(80)	⋯

TABLE X. Summary of numerical results on the F1S ensemble used for the analysis. The values of Z_m are given after interpolation to $\mu = 2$ GeV.

F1S	$10^3 am_{\mathrm{res}}$	aM	Z_A	Z_m^{mSMOM}	Z_m^{SMOM}
0.0021	0.9769(95)	0.0994(18)	0.76231(18)	1.4979(67)	1.5802(18)
0.0043	0.9722(88)	0.1263(13)	0.76263(11)	1.5265(38)	1.5809(18)
0.0107	0.9565(62)	0.18387(86)	0.763139(55)	1.5759(23)	1.5802(17)
0.0214	0.9393(43)	0.25453(57)	0.764180(44)	1.5918(19)	1.5768(17)
0.0330	0.9291(36)	0.31626(41)	0.765486(42)	1.5935(20)	⋯
0.0660	0.9188(24)	0.45975(34)	0.769873(38)	1.5923(19)	⋯
0.0990	0.9251(18)	0.58074(34)	0.775231(37)	1.5822(17)	⋯
0.1320	0.9463(14)	0.68965(34)	0.781619(36)	1.5662(16)	⋯
0.1980	1.0427(11)	0.88429(32)	0.797730(37)	1.5208(13)	⋯
0.2640	1.2577(11)	1.05584(28)	0.818823(38)	1.4630(10)	⋯
0.3300	1.7485(18)	1.20763(25)	0.845736(38)	1.39618(82)	⋯
0.3960	3.1873(46)	1.34062(22)	0.880386(40)	1.31942(65)	⋯

APPENDIX B: MASS CONVERSION FACTOR

Here we determine the mSMOM to $\overline{\text{MS}}$ conversion factor for the mass at one loop in continuum perturbation theory, with an arbitrary choice of the gauge parameter ξ. We work in Minkowski space, with fermion propagator

$$S(p) = \frac{i}{\not{p} - m - \Sigma(p) + i\epsilon}. \tag{B1}$$

We use dimensional regularization in $d = 4 - 2\epsilon$ dimensions, denoting by $\tilde{\mu}$ the dimensionful scale introduced (to distinguish it from the scale μ defining the mSMOM symmetric-momentum point). We compute the fermion self-energy to find the wave function renormalization and then determine Z_m^{mSMOM} by using the mSMOM renormalization from Eq. (2.4), which in Minkowski space reads

$$1 = \frac{1}{12 m_R}\left\{\text{Tr}[-iS_R(p)^{-1}]_{p^2=-\mu^2} - \frac{1}{2}\text{Tr}[q\cdot\Lambda_{\text{A},R}\gamma_5]_{\text{sym}}\right\}. \tag{B2}$$

The conversion factor is given by

$$R_m^{\overline{\text{MS}}\leftarrow\text{mSMOM}} = Z_m^{\overline{\text{MS}}}/Z_m^{\text{mSMOM}}. \tag{B3}$$

The one-loop self-energy integral is

$$-i\Sigma^{(1)}(p) = -g^2\tilde{\mu}^{2\epsilon}C_F\int\frac{d^dk}{(2\pi)^d}\left[\frac{\gamma_\mu(\not{p}-\not{k}+m)\gamma^\mu}{k^2((p-k)^2-m^2)} - (1-\xi)\frac{\not{k}(\not{p}-\not{k}+m)\not{k}}{(k^2)^2((p-k)^2-m^2)}\right], \tag{B4}$$

where $C_F = 4/3$ is the SU(3) quadratic Casimir operator in the fundamental representation. This can be evaluated by standard techniques, using *Mathematica* [49] to perform the Feynman-parameter integrals. The result is

$$\begin{aligned}\Sigma^{(1)}(p) &= \frac{\alpha}{4\pi}C_F\left[\not{p}\xi\left(-\frac{1}{\bar{\epsilon}} - 1 + u + u^2\ln\left(\frac{u}{1+u}\right) + \ln(1+u) + \ln(\mu^2/\tilde{\mu}^2)\right)\right.\\ &\quad\left. + m\left(4 + 2\xi + (3+\xi)\left(\frac{1}{\bar{\epsilon}} + u\ln\left(\frac{u}{1+u}\right) - \ln(1+u) - \ln(\mu^2/\tilde{\mu}^2)\right)\right)\right]\\ &= \frac{\alpha}{4\pi}C_F[\not{p}A_\xi + mB_\xi],\end{aligned} \tag{B5}$$

where we have set $u = m^2/\mu^2$ and have defined

$$\frac{1}{\bar{\epsilon}} \equiv \frac{1}{\epsilon} - \gamma_{\text{E}} + \ln(4\pi). \tag{B6}$$

When $\xi = 1$ the result for $\Sigma^{(1)}(p)$ above agrees with Eq. (37) in Ref. [1]. From this, the mSMOM wave function renormalization constant, up to one loop, is

$$Z_q^{\text{mSMOM}} = 1 - \frac{\alpha}{4\pi}C_F A_\xi. \tag{B7}$$

Now write the one-loop contribution to an amputated bilinear vertex as $\Lambda_\Gamma^{(1)} = \Lambda_{\Gamma,\xi=1}^{(1)} + \Lambda_{\Gamma,\xi\neq1}^{(1)}$, with

$$\Lambda_{\Gamma,\xi=1}^{(1)} = -ig^2\tilde{\mu}^{2\epsilon}C_F\int\frac{d^dk}{(2\pi)^d}\frac{\gamma_\mu(\not{p}_3-\not{k}+m)\Gamma(\not{p}_2-\not{k}+m)\gamma^\mu}{k^2((p_3-k)^2-m^2)((p_2-k)^2-m^2)}, \tag{B8}$$

$$\Lambda_{\Gamma,\xi\neq1}^{(1)} = ig^2\tilde{\mu}^{2\epsilon}C_F(1-\xi)\int\frac{d^dk}{(2\pi)^d}\frac{\not{k}(\not{p}_3-\not{k}+m)\Gamma(\not{p}_2-\not{k}+m)\not{k}/k^2}{k^2((p_3-k)^2-m^2)((p_2-k)^2-m^2)}. \tag{B9}$$

The renormalization condition above requires us to compute $\text{Tr}[q\cdot\Lambda_{\text{A}}^{(1)}\gamma_5]$, with $\Gamma_{\text{A}}^\nu = \gamma^\nu\gamma_5$. By tracing the numerators of the two integrands for $\xi = 1$ and $\xi \neq 1$, we see that

$$\text{Tr}[\Lambda_{\text{A},\xi\neq1}^{(1)}\gamma_5] = -\frac{1-\xi}{d}\text{Tr}[\Lambda_{\text{A},\xi=1}^{(1)}\gamma_5]. \tag{B10}$$

Hence we have to evaluate only the $\xi = 1$ (Feynman gauge) term for $\mathrm{Tr}[\Lambda^{(1)}_{\mathrm{A},\xi=1}\gamma_5]$. Using the notation

$$N_\Gamma = \gamma_\mu(\not{p}_3 - \not{k} + m)\Gamma(\not{p}_2 - \not{k} + m)\gamma^\mu, \tag{B11}$$

we have

$$\mathrm{Tr}[q \cdot N_\mathrm{A}\gamma_5] = 12mdq^2 \tag{B12}$$

and we learn that $\mathrm{Tr}[q \cdot \Lambda^{(1)}_{\mathrm{A},\xi=1}\gamma_5]$ can be expressed in terms of the finite integral

$$-ig^2\tilde{\mu}^{2\epsilon}C_F \int \frac{d^dk}{(2\pi)^d}\frac{1}{k^2((p_3-k)^2-m^2)((p_2-k)^2-m^2)} = -\frac{\alpha}{4\pi}C_F\frac{1}{\mu^2}C_0(m^2/\mu^2), \tag{B13}$$

where $C_0(u)$ comes from a Feynman-parameter integral and is given by

$$C_0(u) = \frac{2i}{\sqrt{3}}\left[\mathrm{Li}_2\left(\frac{-i+\sqrt{3}}{\sqrt{3}-i\sqrt{4u+1}}\right) - \mathrm{Li}_2\left(\frac{i+\sqrt{3}}{\sqrt{3}-i\sqrt{4u+1}}\right) + \mathrm{Li}_2\left(\frac{-i+\sqrt{3}}{i\sqrt{4u+1}+\sqrt{3}}\right) - \mathrm{Li}_2\left(\frac{i+\sqrt{3}}{i\sqrt{4u+1}+\sqrt{3}}\right)\right]. \tag{B14}$$

Since the result is finite, we can set $d = 4$ and find

$$\mathrm{Tr}[q \cdot \Lambda^{(1)}_\mathrm{A}\gamma_5]_\mathrm{sym} = \left(1 - \frac{1-\xi}{4}\right)\mathrm{Tr}[q \cdot \Lambda^{(1)}_{\mathrm{A},\xi=1}\gamma_5]_\mathrm{sym} = 12m\frac{\alpha}{4\pi}C_F(3+\xi)C_0(m^2/\mu^2). \tag{B15}$$

Now we have all we need to evaluate Z_m^{mSMOM} from the renormalization condition in (B2), which we rewrite as

$$Z_m^{\mathrm{mSMOM}} = \lim_{m_\mathrm{R}\to\bar{m}}\frac{1}{12m}\frac{1}{Z_q^{\mathrm{mSMOM}}}\left[\mathrm{Tr}(-iS(p)^{-1})_{p^2=-\mu^2} - \frac{1}{2}Z_\mathrm{A}^{\mathrm{mSMOM}}\mathrm{Tr}(q \cdot \Lambda_\mathrm{A}\gamma_5)_\mathrm{sym}\right]. \tag{B16}$$

Using the results in (B5), (B7) and (B15), together with (in Minkowski space) $iS(p)^{-1} = \not{p} - m - \Sigma(p)$, shows that to one loop,

$$\begin{aligned} Z_m^{\mathrm{mSMOM}} &= 1 + \frac{\alpha}{4\pi}C_F\left[A_\xi + B_\xi - \frac{3+\xi}{2}C_0(\bar{m}^2/\mu^2)\right] \\ &= 1 + \frac{\alpha}{4\pi}C_F\left[3\frac{1}{\bar{\epsilon}} + (4+\xi) - \frac{3+\xi}{2}C_0(u) - 3\ln(\mu^2/\tilde{\mu}^2)\right. \\ &\quad \left. + \xi\left(u + u^2\ln\left(\frac{u}{1+u}\right)\right) + (3+\xi)u\ln\left(\frac{u}{1+u}\right) - 3\ln(1+u)\right], \end{aligned} \tag{B17}$$

where now $u = \bar{m}^2/\mu^2$. Finally, the conversion factor is

$$\begin{aligned} R_m^{\overline{\mathrm{MS}}\leftarrow\mathrm{mSMOM}} &= 1 + \frac{\alpha}{4\pi}C_F\left[-(4+\xi) + \frac{3+\xi}{2}C_0(u) + 3\ln(\mu^2/\tilde{\mu}^2) + 3\ln(1+u)\right. \\ &\quad \left. - \xi\left(u + u^2\ln\left(\frac{u}{1+u}\right)\right) - (3+\xi)u\ln\left(\frac{u}{1+u}\right)\right]. \end{aligned} \tag{B18}$$

When $\bar{m} \to 0$ ($u \to 0$), this agrees with Eq. (24) in Sturm *et al.* [3], after setting $\tilde{\mu} = \mu$. For $\xi = 1$ the result for $Z_\mathrm{P}^{\mathrm{mSMOM}} = 1/Z_m^{\mathrm{mSMOM}}$ reproduces the Feynman-gauge result in Ref. [1]. We also computed $Z_\mathrm{P}^{\mathrm{mSMOM}}$ to one-loop order directly from the renormalization condition of Eq. (2.7) (in Minkowski space) and confirmed that $Z_\mathrm{P}^{\mathrm{mSMOM}} = 1/Z_m^{\mathrm{mSMOM}}$ for arbitrary ξ.

The lattice computations are performed using Landau-gauge-fixed configurations and hence we need the conversion factor in Landau gauge, $\xi = 0$,

$$R_m^{\overline{\mathrm{MS}}\leftarrow\mathrm{mSMOM}} = 1 + \frac{\alpha}{4\pi}C_F\left[-4 + \frac{3}{2}C_0(u) + 3\ln(\mu^2/\tilde{\mu}^2) + 3\ln(1+u) - 3u\ln\left(\frac{u}{1+u}\right)\right]. \tag{B19}$$

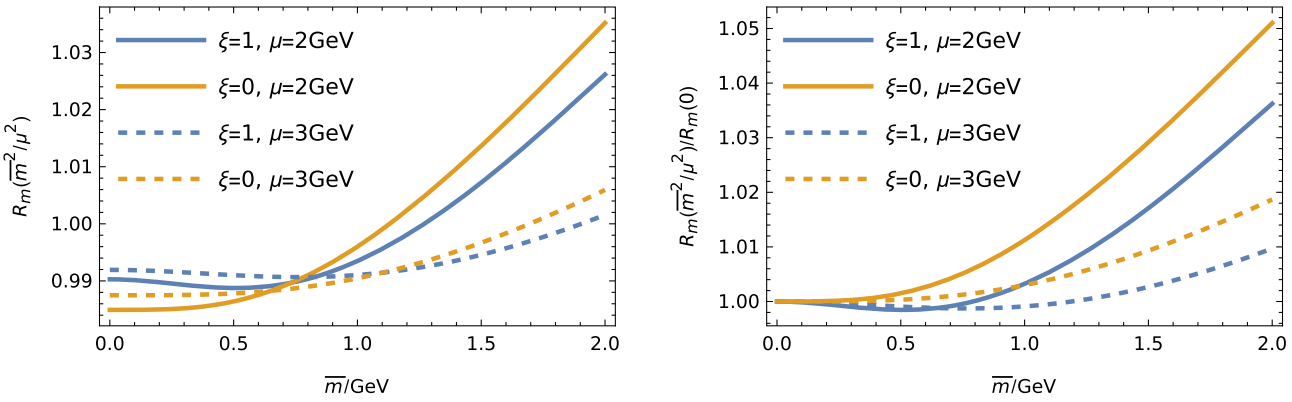

FIG. 10. Conversion factors between the mSMOM and $\overline{\text{MS}}$ and the mSMOM and SMOM schemes. Left: conversion factor $R_m^{\overline{\text{MS}}\leftarrow\text{mSMOM}}(m^2/\mu^2)$ for $0 < m < 2$ GeV. Right: ratio $R_m^{\overline{\text{MS}}\leftarrow\text{mSMOM}}(m^2/\mu^2)/R_m^{\overline{\text{MS}}\leftarrow\text{mSMOM}}(0) = R_m^{\text{SMOM}\leftarrow\text{mSMOM}}(m^2/\mu^2)$. Both plots show curves with $(\alpha, \mu) = (0.293347, 2\text{ GeV})$ (solid) and $(\alpha, \mu) = (0.24358, 3\text{ GeV})$ (dashed) and for gauge parameter ξ set to 1 (Feynman gauge) or 0 (Landau gauge). The dimensional regularization scale $\tilde{\mu}$ is set to μ.

In Fig. 10, we show plots of the mass conversion factor as a function of $\bar{m}$, in both Feynman and Landau gauge for two choices of matching scale μ (taking $\tilde{\mu} = \mu$).

[1] Peter Boyle, Luigi Del Debbio, and Ava Khamseh, Massive momentum-subtraction scheme, Phys. Rev. D **95**, 054505 (2017).

[2] Luigi Del Debbio, Felix Erben, Jonathan Flynn, Rajnandini Mukherjee, and J. Tobias Tsang, Charm quark mass using a massive nonperturbative renormalisation scheme, Proc. Sci. LATTICE2023 (**2024**) 294 [arXiv:2312.16537].

[3] C. Sturm, Y. Aoki, N. H. Christ, T. Izubuchi, C. T. C. Sachrajda *et al.*, Renormalization of quark bilinear operators in a momentum-subtraction scheme with a non-exceptional subtraction point, Phys. Rev. D **80**, 014501 (2009).

[4] G. Martinelli, C. Pittori, Christopher T. Sachrajda, M. Testa, and A. Vladikas, A general method for nonperturbative renormalization of lattice operators, Nucl. Phys. **B445**, 81 (1995).

[5] Y. Aoki *et al.*, Continuum limit of B_K from $2+1$ flavor domain wall QCD, Phys. Rev. D **84**, 014503 (2011).

[6] T. Blum *et al.* (RBC, UKQCD Collaborations), Domain wall QCD with physical quark masses, Phys. Rev. D **93**, 074505 (2016).

[7] Peter A. Boyle, Luigi Del Debbio, Andreas Jüttner, Ava Khamseh, Francesco Sanfilippo, and Justus Tobias Tsang, The decay constants $\mathbf{f_D}$ and $\mathbf{f_{D_s}}$ in the continuum limit of $\mathbf{N_f = 2 + 1}$ domain wall lattice QCD, J. High Energy Phys. 12 (2017) 008.

[8] Peter A. Boyle, Luigi Del Debbio, Nicolas Garron, Andreas Juttner, Amarjit Soni, Justus Tobias Tsang, and Oliver Witzel (RBC/UKQCD Collaborations), SU(3)-breaking ratios for $D_{(s)}$ and $B_{(s)}$ mesons, arXiv:1812.08791.

[9] Peter A. Boyle, Felix Erben, Jonathan M. Flynn, Nicolas Garron, Julia Kettle, Rajnandini Mukherjee, and J. Tobias Tsang, Kaon mixing beyond the standard model with physical masses, Phys. Rev. D **110**, 034501 (2024).

[10] Y. Iwasaki and T. Yoshie, Renormalization group improved action for SU(3) lattice gauge theory and the string tension, Phys. Lett. **143B**, 449 (1984).

[11] Y. Iwasaki, Renormalization group analysis of lattice theories and improved lattice action: Two-dimensional nonlinear O(N) sigma model, Nucl. Phys. **B258**, 141 (1985).

[12] Yigal Shamir, Chiral fermions from lattice boundaries, Nucl. Phys. **B406**, 90 (1993).

[13] Vadim Furman and Yigal Shamir, Axial symmetries in lattice QCD with Kaplan fermions, Nucl. Phys. **B439**, 54 (1995).

[14] Richard C. Brower, Hartmut Neff, and Kostas Orginos, Mobius fermions: Improved domain wall chiral fermions, Nucl. Phys. B, Proc. Suppl. **140**, 686 (2005).

[15] R. C. Brower, H. Neff, and K. Orginos, Mobius fermions, Nucl. Phys. B, Proc. Suppl. **153**, 191 (2006).

[16] Richard C. Brower, Harmut Neff, and Kostas Orginos, The Möbius domain wall fermion algorithm, Comput. Phys. Commun. **220**, 1 (2017).

[17] Peter Boyle, Andreas Juttner, Marina Krstic Marinkovic, Francesco Sanfilippo, Matthew Spraggs, and Justus Tobias Tsang, An exploratory study of heavy domain wall fermions on the lattice, J. High Energy Phys. 04 (2016) 037.

[18] Peter A. Boyle, Guido Cossu, Azusa Yamaguchi, and Antonin Portelli, Grid: A next generation data parallel C++ QCD library, Proc. Sci. LATTICE2015 (**2016**) 023.

[19] Azusa Yamaguchi, Peter Boyle, Guido Cossu, Gianluca Filaci, Christoph Lehner, and Antonin Portelli, Grid: One-Code and FourAPIs, Proc. Sci. LATTICE2021 (**2022**) 035 [arXiv:2203.06777].

[20] Antonin Portelli, Nelson Lachini, Felix Erben, Michael Marshall, Fabian Joswig, Raoul Hodgson, Fionn Ó hÓgáin, Vera Gülpers, Peter Boyle, Nils Asmussen, Ryan Hill, Alessandro Barone, James Richings, Ryan Abbott, Simon Bürger, and Joseph Lee, aportelli/hadrons: Hadrons v1.4 (2023), 10.5281/zenodo.8023716.
[21] T. Blum, P. Chen, Norman H. Christ, C. Cristian, C. Dawson *et al.*, Quenched lattice QCD with domain wall fermions and the chiral limit, Phys. Rev. D **69**, 074502 (2004).
[22] P. A. Boyle, Conserved currents for Mobius domain wall fermions, arXiv:1411.5728.
[23] C. T. H. Davies, C. McNeile, E. Follana, G. P. Lepage, H. Na, and J. Shigemitsu, Update: Precision D_s decay constant from full lattice QCD using very fine lattices, Phys. Rev. D **82**, 114504 (2010).
[24] R. L. Workman *et al.* (Particle Data Group), Review of particle physics, Prog. Theor. Exp. Phys. **2022**, 083C01 (2022).
[25] Martin Gorbahn and Sebastian Jager, Precise MS-bar light-quark masses from lattice QCD in the RI/SMOM scheme, Phys. Rev. D **82**, 114001 (2010).
[26] Leandro G. Almeida and Christian Sturm, Two-loop matching factors for light quark masses and three-loop mass anomalous dimensions in the RI/SMOM schemes, Phys. Rev. D **82**, 054017 (2010).
[27] K. G. Chetyrkin, Johann H. Kuhn, and M. Steinhauser, RunDec: A *Mathematica* package for running and decoupling of the strong coupling and quark masses, Comput. Phys. Commun. **133**, 43 (2000).
[28] Barbara Schmidt and Matthias Steinhauser, CRunDec: A C++ package for running and decoupling of the strong coupling and quark masses, Comput. Phys. Commun. **183**, 1845 (2012).
[29] Florian Herren and Matthias Steinhauser, Version 3 of RunDec and CRunDec, Comput. Phys. Commun. **224**, 333 (2018).
[30] P. A. Baikov, K. G. Chetyrkin, and J. H. Kühn, Quark mass and field anomalous dimensions to $\mathcal{O}(\alpha_s^5)$, J. High Energy Phys. 10 (2014) 076.
[31] Thomas Luthe, Andreas Maier, Peter Marquard, and York Schröder, Five-loop quark mass and field anomalous dimensions for a general gauge group, J. High Energy Phys. 01 (2017) 081.
[32] P. A. Baikov, K. G. Chetyrkin, and J. H. Kühn, Five-loop fermion anomalous dimension for a general gauge group from four-loop massless propagators, J. High Energy Phys. 04 (2017) 119.
[33] P. A. Baikov, K. G. Chetyrkin, and J. H. Kühn, Five-loop running of the QCD coupling constant, Phys. Rev. Lett. **118**, 082002 (2017).
[34] F. Herzog, B. Ruijl, T. Ueda, J. A. M. Vermaseren, and A. Vogt, The five-loop beta function of Yang-Mills theory with fermions, J. High Energy Phys. 02 (2017) 090.
[35] Thomas Luthe, Andreas Maier, Peter Marquard, and York Schroder, Complete renormalization of QCD at five loops, J. High Energy Phys. 03 (2017) 020.
[36] Y. Aoki *et al.* (Flavour Lattice Averaging Group (FLAG) Collaboration), FLAG review 2021, Eur. Phys. J. C **82**, 869 (2022).
[37] Jochen Heitger, Fabian Joswig, and Simon Kuberski (ALPHA Collaboration), Determination of the charm quark mass in lattice QCD with $2+1$ flavors on fine lattices, J. High Energy Phys. 05 (2021) 288.
[38] P. Petreczky and J. H. Weber, Strong coupling constant and heavy quark masses in $(2+1)$ -flavor QCD, Phys. Rev. D **100**, 034519 (2019).
[39] Katsumasa Nakayama, Brendan Fahy, and Shoji Hashimoto, Short-distance charmonium correlator on the lattice with Möbius domain-wall fermion and a determination of charm quark mass, Phys. Rev. D **94**, 054507 (2016).
[40] Yi-Bo Yang *et al.*, Charm and strange quark masses and f_{D_s} from overlap fermions, Phys. Rev. D **92**, 034517 (2015).
[41] C. McNeile, C. T. H. Davies, E. Follana, K. Hornbostel, and G. P. Lepage, High-precision c and b masses, and QCD coupling from current-current correlators in lattice and continuum QCD, Phys. Rev. D **82**, 034512 (2010).
[42] C. Alexandrou *et al.* (Extended Twisted Mass Collaboration), Quark masses using twisted-mass fermion gauge ensembles, Phys. Rev. D **104**, 074515 (2021).
[43] D. Hatton, C. T. H. Davies, B. Galloway, J. Koponen, G. P. Lepage, and A. T. Lytle (HPQCD Collaboration), Charmonium properties from lattice $QCD+\mathrm{QED}$: Hyperfine splitting, J/ψ leptonic width, charm quark mass, and a_μ^c, Phys. Rev. D **102**, 054511 (2020).
[44] A. Bazavov *et al.* (Fermilab Lattice, MILC, TUMQCD Collaborations), Up-, down-, strange-, charm-, and bottom-quark masses from four-flavor lattice QCD, Phys. Rev. D **98**, 054517 (2018).
[45] C. Alexandrou, V. Drach, K. Jansen, C. Kallidonis, and G. Koutsou, Baryon spectrum with $N_f = 2+1+1$ twisted mass fermions, Phys. Rev. D **90**, 074501 (2014).
[46] Bipasha Chakraborty, C. T. H. Davies, B. Galloway, P. Knecht, J. Koponen, G. C. Donald, R. J. Dowdall, G. P. Lepage, and C. McNeile, High-precision quark masses and QCD coupling from $n_f = 4$ lattice QCD, Phys. Rev. D **91**, 054508 (2015).
[47] N. Carrasco *et al.* (European Twisted Mass Collaboration), Up, down, strange and charm quark masses with $\mathrm{N}_f = 2+1+1$ twisted mass lattice QCD, Nucl. Phys. **B887**, 19 (2014).
[48] Andrea Bussone, Alessandro Conigli, Julien Frison, Gregorio Herdoíza, Carlos Pena, David Preti, Alejandro Sáez, and Javier Ugarrio (Alpha Collaboration), Hadronic physics from a Wilson fermion mixed-action approach: Charm quark mass and $D_{(s)}$ meson decay constants, Eur. Phys. J. C **84**, 506 (2024).
[49] Mathematica, Version 14.0 (Wolfram Research Inc., Champaign, IL, 2024).